

Electronic Supplementary Information for:

# Ligand Control of Low-Frequency Electron Paramagnetic Resonance Linewidth in Cr(III) Complexes

Anthony C. Campanella,<sup>a</sup> Manh-Thuong Nguyen,<sup>b</sup> Jun Zhang,<sup>b</sup> Thacien  
Ngendahimana,<sup>c</sup> William E. Antholine,<sup>d</sup> Gareth R. Eaton,<sup>c</sup> Sandra S. Eaton,<sup>c</sup>  
Vassiliki-Alexandra Glezakou,<sup>b</sup> and Joseph M. Zadrozny\*<sup>a</sup>

<sup>a</sup>Department of Chemistry, Colorado State University, Fort Collins, Colorado 80523, USA.

<sup>b</sup>Physical Sciences Division, Pacific Northwest National Laboratory, Richland, Washington 99354, USA.

<sup>c</sup>Department of Chemistry and Biochemistry, University of Denver, Denver, CO 80208, USA

<sup>d</sup>Biophysics Research Institute, Medical College of Wisconsin, Milwaukee, Wisconsin 53226, USA.

## Table of Contents

Description	Page
<b>Full Experimental Details.</b>	<b>S3</b>
<b>Table S1.</b> Crystallographic information for the structural refinement of <b>1</b> .	<b>S12</b>
<b>Table S2.</b> Crystallographic information for the structural refinement of <b>4</b> .	<b>S13</b>
<b>Table S3.</b> Crystallographic information for the structural refinement of <b>5-RR</b> .	<b>S14</b>
<b>Table S4.</b> Crystallographic information for the structural refinement of <b>5-SS</b> .	<b>S15</b>
<b>Table S5.</b> Selected inner coordination sphere bond lengths and angles of <b>1</b> .	<b>S16</b>
<b>Table S6.</b> Selected inner coordination sphere bond lengths and angles of <b>1</b> .	<b>S16</b>
<b>Table S7.</b> Selected inner coordination sphere bond lengths and angles of <b>5-RR</b> .	<b>S16</b>
<b>Table S8.</b> Selected inner coordination sphere bond lengths and angles of <b>5-SS</b> .	<b>S17</b>
<b>Table S9.</b> Continuous-shape-measurement (CSM) analysis results for <b>1-5</b> .	<b>S17</b>
<b>Table S10.</b> Fluorescent lifetimes for <b>1-5</b> .	<b>S17</b>
<b>Table S11.</b> Spin Hamiltonian parameters for <b>1-5</b> .	<b>S18</b>
<b>Fig. S1.</b> Thermal ellipsoid plot of <b>1</b> .	<b>S19</b>
<b>Fig. S2.</b> Thermal ellipsoid plot of <b>4</b> .	<b>S20</b>
<b>Fig. S3.</b> Thermal ellipsoid plot of <b>5-RR</b> .	<b>S21</b>
<b>Fig. S4.</b> Thermal ellipsoid plot of <b>5-SS</b> .	<b>S22</b>
<b>Fig. S5.</b> CW X-band EPR spectra of <b>1-5</b> .	<b>S23</b>
<b>Fig. S6.</b> Electronic absorption spectroscopy data for <b>1-5</b> .	<b>S24</b>
<b>Fig. S7.</b> Electronic absorption spectroscopy data for <b>5</b> , <b>5-SS</b> , <b>5-RR</b> .	<b>S25</b>
<b>Fig. S8.</b> Steady-state electronic emission spectroscopy data for <b>1-5</b> .	<b>S26</b>
<b>Fig. S9.</b> Steady-state electronic emission spectroscopy data for <b>5</b> , <b>5-SS</b> , <b>5-RR</b> .	<b>S27</b>
<b>Fig. S10.</b> Time-resolved emission spectroscopy data for <b>1</b> , <b>3</b> , <b>4</b> .	<b>S28</b>
<b>Fig. S11.</b> Time-resolved emission spectroscopy data for <b>2</b> , and <b>5</b> .	<b>S28</b>
<b>Fig. S12.</b> Time-resolved emission spectroscopy data for <b>5</b> ligand.	<b>S29</b>
<b>Fig. S13.</b> L-band CW EPR spectra for <b>5</b> and <b>5-SS</b> .	<b>S30</b>
<b>Fig. S14.</b> Optimized structures of <b>1</b> , <b>2</b> , <b>4</b> , and <b>5</b> with local waters.	<b>S31</b>
<b>Fig. S15.</b> MD simulation boxes for <b>1</b> , <b>2</b> , <b>4</b> , and <b>5</b> .	<b>S31</b>
<b>References</b>	<b>S32</b>

## Full Experimental Details

**General Considerations.** Reagents used throughout were purchased from commercial sources and used as received. Syntheses were adapted from a previously reported procedure.<sup>1</sup> All techniques were performed at atmospheric conditions unless otherwise specified.

**[Cr(*RR*-dphen)<sub>3</sub>]Cl<sub>3</sub>•EtOH (1)** In a 5 mL round-bottom flask, 160 mg of CrCl<sub>3</sub>•6H<sub>2</sub>O (0.602 mmol, 1 eq.) were added to 0.5 mL of dimethyl sulfoxide (DMSO) and heated to 200°C with stirring. Upon reaching temperature, the mixture was cooled to 110°C. While that mixture cooled, 400 mg (1.88 mmol, 3.1 eq.) of (1*R*,2*R*)-(+)-1,2-diphenylethylenediamine were placed in a vial with ca. 0.5 mL of DMSO and warmed until dissolved. The diamine solution was added to the CrCl<sub>3</sub> solution and the temperature was raised to 150°C for 1 hour, then allowed to cool to room temperature. A small amount of a dark yellow powder was visible. 1 mL of ethanol followed by 1 mL of ethyl ether were added to encourage precipitation. The solid was filtered, washed once with 5 mL of ethanol, then three times with 5 mL of ethyl ether, yielding a shiny, yellow-orange microcrystalline powder. This solid was further purified by recrystallization from aqueous ethanol and dried under vacuum. The final yield was 125.7 mg (26%) of **1**. Crystals suitable for single-crystal x-ray diffraction were grown by the slow evaporation of a saturated methanol solution of **1**. IR (cm<sup>-1</sup>, diamond ATR): 3032, 2905, 1579, 1497, 1455, 1401, 1310, 1238, 1180, 1076, 1024, 1000, 952, 915, 867, 764, 699. UV-vis (H<sub>2</sub>O); λ<sub>max</sub> (ε<sub>M</sub>, M<sup>-1</sup>cm<sup>-1</sup>): 354 nm (85.7); 464 nm (94.5). LC-MS (m/z): positive ion mode: {[Cr(*RR*-dphen)<sub>3</sub>Cl<sub>2</sub>]}<sup>+</sup>, 758.27; {[Cr(*RR*-dphen)<sub>2</sub>Cl]}<sup>++</sup>, 214.63. Elemental analysis for C<sub>42</sub>H<sub>48</sub>Cl<sub>3</sub>CrN<sub>6</sub>•C<sub>2</sub>H<sub>6</sub>O calculated (found): %C: 62.82 (62.88), %H: 6.47 (6.39), %N: 9.99 (9.72).

**[Cr(en)<sub>3</sub>]Cl<sub>3</sub> (2)** In a 50 mL round-bottom flask, 4 g of CrCl<sub>3</sub>•6H<sub>2</sub>O (15 mmol, 1 eq.) were added to 8 mL of dimethyl sulfoxide (DMSO) and heated to 200°C with stirring. Upon reaching temperature, the mixture was cooled to 110°C. While that mixture cooled, 4 mL (60 mmol, 4 eq.) of anhydrous ethylenediamine were placed in a vial with ca. 2 mL of DMSO and warmed. The diamine solution was added to the CrCl<sub>3</sub> solution and the temperature was raised to 150°C for 1 hour, then allowed to cool to room temperature. A small amount of a dark yellow powder was visible. 5 mL of ethanol and 2 mL of ethyl ether were added to encourage precipitation. The solid was filtered, washed several times with 10 mL of ethanol, then once with 10 mL of ethyl ether, yielding a shiny, yellow-orange microcrystalline powder. This solid was further purified by recrystallization from aqueous ethanol and dried under vacuum. The final yield was 4.63 g (91%)

of **2**. IR ( $\text{cm}^{-1}$ , diamond ATR): 3180, 3121, 3066, 2984, 2950, 2938, 2898, 2890, 1575, 1560, 1537, 1459, 1364, 1331, 1304, 1275, 1214, 1158, 1141, 1121, 1059, 1010, 881, 867, 745. UV-vis ( $\text{H}_2\text{O}$ ) spectra matches prior reports<sup>1</sup>;  $\lambda_{\text{max}}$  ( $\epsilon_{\text{M}}$ ,  $\text{M}^{-1}\text{cm}^{-1}$ ): 351 nm (60.6); 458 nm (76.5). LC-MS ( $m/z$ ): positive ion mode:  $\{[\text{Cr}(\text{en})_3\text{Cl}_2]\}^+$ , 302.08;  $\{[\text{Cr}(\text{en})_2\text{Cl}_2]\}^+$ , 242.01. Elemental analysis for  $\text{C}_6\text{H}_{24}\text{Cl}_3\text{CrN}_6$  calculated (found): %C: 21.28 (21.26), %H: 7.14 (7.17), %N: 24.82 (24.47).

**[Cr(me-en)<sub>3</sub>]Cl<sub>3</sub>•0.25H<sub>2</sub>O (3)** In a 50 mL round-bottom flask, 4 g of  $\text{CrCl}_3\cdot 6\text{H}_2\text{O}$  (15 mmol, 1 eq.) were added to 8 mL of dimethyl sulfoxide (DMSO) and heated to 200°C with stirring. Upon reaching temperature, the mixture was cooled to 110°C. While that mixture cooled, 5 mL (59 mmol, 3.9 eq.) of 1,2-propanediamine were placed in a vial with ca. 2 mL of DMSO and warmed. The diamine solution was added to the  $\text{CrCl}_3$  solution and the temperature was raised to 150°C for 1 hour, then allowed to cool to room temperature. A small amount of a dark yellow powder was visible. 5 mL of ethanol and 2 mL of ethyl ether were added to encourage precipitation. The solid was filtered, washed three times with 10 mL of ethanol, then once with 10 mL of ethyl ether, yielding a yellow-orange powder. This solid was further purified by recrystallization from aqueous ethanol and dried under vacuum. The final yield was 2.98 g (58%) of **3**. IR ( $\text{cm}^{-1}$ , diamond ATR): 3163, 3054, 2965, 2938, 2880, 1538, 1456, 1393, 1372, 1343, 1310, 1236, 1126, 1101, 1042, 1015, 836, 730. UV-vis ( $\text{H}_2\text{O}$ ) matches reported spectra<sup>2</sup>;  $\lambda_{\text{max}}$  ( $\epsilon_{\text{M}}$ ,  $\text{M}^{-1}\text{cm}^{-1}$ ): 352 nm (59.5); 459 nm (74.1). LC-MS ( $m/z$ ): positive ion mode:  $\{[\text{Cr}(\text{me-en})_3\text{Cl}_2]\}^+$ , 344.13;  $\{[\text{Cr}(\text{me-en})_2\text{Cl}_2]\}^+$ , 270.04. Elemental analysis for  $\text{C}_9\text{H}_{30}\text{Cl}_3\text{CrN}_6\cdot 0.25\text{H}_2\text{O}$  calculated (found): %C: 28.06 (28.21), %H: 7.98 (8.13), %N: 21.82 (21.65).

**[Cr(tn)<sub>3</sub>]Cl<sub>3</sub> (4)** In a 50 mL round-bottom flask, 4 g of  $\text{CrCl}_3\cdot 6\text{H}_2\text{O}$  (15 mmol, 1 eq.) were added to 8 mL of dimethyl sulfoxide (DMSO) and heated to 200°C with stirring. Upon reaching temperature, the mixture was cooled to 110°C. While that mixture cooled, 8 mL (94 mmol, 6.2 eq.) of 1,3-diaminopropane were placed in a vial with ca. 2 mL of DMSO and warmed. The diamine solution was added to the  $\text{CrCl}_3$  solution and the temperature was raised to 150°C for 1 hour, then allowed to cool to room temperature. A small amount of a dark yellow powder was visible. 5 mL of ethanol and 2 mL of ethyl ether were added to encourage precipitation. The solid was filtered, washed three times with 10 mL of ethanol, then once with 10 mL of ethyl ether, yielding a shiny, yellow-orange microcrystalline powder. This solid was further purified by recrystallization from aqueous ethanol and dried under vacuum. The final yield was 2.53 g (49%) of **4**. Single crystals suitable for single-crystal X-ray diffraction were grown from layering ethanol

onto an aqueous solution of **4**. IR (cm<sup>-1</sup>, diamond ATR): 3277, 3129, 3072, 3032, 2960, 2942, 2946, 2887, 1596, 1568, 1546, 1479, 1464, 1444, 1401, 1390, 1352, 1303, 1285, 1259, 1228, 1218, 1186, 1171, 1034, 1025, 932, 917, 897, 877, 806, 731, 691, 673. UV-vis (H<sub>2</sub>O) matches prior reports<sup>1</sup>; λ<sub>max</sub> (ε<sub>M</sub>, M<sup>-1</sup>cm<sup>-1</sup>): 355 nm (47.2); 464 nm (55.3). LC-MS (m/z): positive ion mode: {[Cr(tn)<sub>3</sub>Cl<sub>2</sub>]}<sup>+</sup>, 344.13; {[Cr(tn)<sub>2</sub>Cl<sub>2</sub>]}<sup>+</sup>, 270.04. Elemental analysis for C<sub>9</sub>H<sub>30</sub>Cl<sub>3</sub>CrN<sub>6</sub> calculated (found): %C: 28.39 (28.36), %H: 7.94 (8.06), %N: 22.07 (21.89).

**[Cr(*trans*-chxn)<sub>3</sub>]Cl<sub>3</sub>•0.25H<sub>2</sub>O•0.25EtOH (5)** In a 25 mL round-bottom flask, 1.5 g of CrCl<sub>3</sub>•6H<sub>2</sub>O (5.63 mmol, 1 eq.) were added to 4 mL of dimethyl sulfoxide (DMSO) and heated to 200°C with stirring. Upon reaching temperature, the mixture was cooled to 110°C. While that mixture cooled, 2.7 mL (22.5 mmol, 4 eq.) of *trans*-1,2-diaminocyclohexane were placed in a vial with ca. 1 mL of DMSO and warmed. The diamine solution was added to the CrCl<sub>3</sub> solution and the temperature was raised to 150°C for 1 hour, then allowed to cool to room temperature. A small amount of a dark yellow powder was visible. 4 mL of ethanol and 2 mL of ethyl ether were added to encourage precipitation. The solid was filtered, washed three times with 10 mL ethanol, then once with 10 mL ethyl ether, yielding a shiny, yellow-orange microcrystalline powder. This solid was further purified by recrystallization from aqueous ethanol and dried under vacuum. The final yield was 1.25 g (44%) of **5**. IR (cm<sup>-1</sup>, diamond ATR): 3041, 2933, 2864, 1590, 1574, 1459, 1449, 1409, 1397, 1359, 1303, 1240, 1211, 1152, 1122, 1051, 1024, 946, 921, 859, 751. UV-vis (H<sub>2</sub>O) match reported data<sup>1</sup>; λ<sub>max</sub> (ε<sub>M</sub>, M<sup>-1</sup>cm<sup>-1</sup>): 352 nm (55.9); 460 nm (71.1). LC-MS (m/z): positive ion mode: {[Cr(*trans*-chxn)<sub>3</sub>Cl<sub>2</sub>]}<sup>+</sup>, 464.22; {[Cr(*trans*-chxn)<sub>2</sub>Cl<sub>2</sub>]}<sup>+</sup>, 350.10; {[Cr(*trans*-chxn)<sub>2</sub>Cl]}<sup>++</sup>, 214.63. Elemental analysis for C<sub>18</sub>H<sub>42</sub>Cl<sub>3</sub>CrN<sub>6</sub>•0.25H<sub>2</sub>O•0.25C<sub>2</sub>H<sub>6</sub>O calculated (found): %C: 42.98 (42.90), %H: 8.58 (8.94), %N: 16.26 (16.53).

**[Cr(*SS*-chxn)<sub>3</sub>]Cl<sub>3</sub>•H<sub>2</sub>O (5-*SS*)** In a 25 mL round-bottom flask, 707 mg of CrCl<sub>3</sub>•6H<sub>2</sub>O (2.65 mmol, 1 eq.) were added to 2 mL of dimethyl sulfoxide (DMSO) and heated to 200°C with stirring. Upon reaching temperature, the mixture was cooled to 110°C. While that mixture cooled, 1 g (8.76 mmol, 3.3 eq.) of (*1S,2S*)-(+)-1,2-diaminocyclohexane were placed in a vial with ca. 1 mL of DMSO and warmed. The diamine solution was added to the CrCl<sub>3</sub> solution and the temperature was raised to 150°C for 1 hour, then allowed to cool to room temperature. A small amount of a dark yellow powder was visible. 2 mL of ethanol and 1 mL of ethyl ether were added to encourage precipitation. The solid was filtered, washed three times with 5 mL of ethanol, then once with 5 mL of ethyl ether, yielding a shiny, yellow-orange microcrystalline powder. This solid was further

purified by recrystallization from aqueous ethanol and dried under vacuum. The final yield was 539 mg (40%) of **5-SS**. Crystals suitable for single crystal x-ray diffraction were grown through the slow evaporation of a saturated aqueous solution of **5-SS**. IR (cm<sup>-1</sup>, diamond ATR): 3138, 3036, 2930, 2857, 1576, 1448, 1401, 1364, 1346, 1303, 1240, 1211, 1145, 1051, 1020, 948, 919, 862, 754. UV-vis (H<sub>2</sub>O) match reported data<sup>1</sup>; λ<sub>max</sub> (ε<sub>M</sub>, M<sup>-1</sup>cm<sup>-1</sup>): 352 nm (65.7); 461 nm (83.6). LC-MS (m/z): positive ion mode: {[Cr(SS-chxn)<sub>3</sub>Cl<sub>2</sub>]}<sup>+</sup>, 464.22; {[Cr(SS-chxn)<sub>2</sub>Cl<sub>2</sub>]}<sup>+</sup>, 350.10; {[Cr(SS-chxn)<sub>2</sub>Cl]}<sup>++</sup>, 214.63. Elemental analysis for CrC<sub>18</sub>H<sub>42</sub>Cl<sub>3</sub>N<sub>6</sub>•H<sub>2</sub>O calculated (found): %C: 41.66 (41.69), %H: 8.55 (8.88), %N: 16.19 (15.81).

**[Cr(RR-chxn)<sub>3</sub>]Cl<sub>3</sub>•0.75H<sub>2</sub>O•0.25EtOH (5-RR)** In a 25 mL round-bottom flask, 707 mg of CrCl<sub>3</sub>•6H<sub>2</sub>O (2.65 mmol, 1 eq.) were added to 2 mL of dimethyl sulfoxide (DMSO) and heated to 200°C with stirring. Upon reaching temperature, the mixture was cooled to 110°C. While that mixture cooled, 1 g (8.76 mmol, 3.3 eq.) of (1*R*,2*R*)-(-)-1,2-diaminocyclohexane were placed in a vial with ca. 1 mL of DMSO and warmed. The diamine solution was added to the CrCl<sub>3</sub> solution and the temperature was raised to 150°C for 1 hour, then allowed to cool to room temperature. A small amount of a dark yellow powder was visible. 2 mL of ethanol and 1 mL of ethyl ether were added to encourage precipitation. The solid was filtered, washed three times with 5 mL of ethanol, then once with 5 mL of ethyl ether, yielding a shiny, yellow-orange microcrystalline powder. This solid was further purified by recrystallization from aqueous ethanol and dried under vacuum. The final yield was 812 mg (60%) of **5-RR**. Crystals suitable for single crystal x-ray diffraction were grown through the slow evaporation of a saturated aqueous solution of **5-RR**. IR (cm<sup>-1</sup>, diamond ATR): 3141, 3038, 2932, 2857, 1576, 1450, 1402, 1366, 1345, 1304, 1240, 1211, 1146, 1050, 1020, 949, 919, 862, 754. UV-vis (H<sub>2</sub>O) match reported data<sup>1</sup>; λ<sub>max</sub> (ε<sub>M</sub>, M<sup>-1</sup>cm<sup>-1</sup>): 352 nm (74.5); 460 nm (93.0). Elemental analysis for C<sub>18</sub>H<sub>42</sub>Cl<sub>3</sub>CrN<sub>6</sub>•0.75H<sub>2</sub>O•0.25C<sub>2</sub>H<sub>6</sub>O calculated (found): %C: 42.25 (42.26), %H: 8.62 (8.38), %N: 15.98 (15.98).

**X-ray Data Collection, Structure Solution and Refinement for 1, 4, and 5-SS, 5-RR.** The diffraction data were collected at the X-Ray Diffraction facility of the Analytical Resources COre at Colorado State University. Data for **1**, **4**, **5-SS**, and **5-RR** were collected on a Bruker D8 Quest ECO single-crystal X-ray diffractometer equipped with Mo Kα (λ = 0.71073 Å). Data were collected and integrated using Bruker Apex 3 software. Absorption correction were applied using SADABS.<sup>3</sup> Space group assignments were determined by examination of systematic absences, E-

statistics, and successive refinement of the structures. Crystal structures were solved using SHELXT and refined with the aid of successive difference Fourier maps by SHELXL operated in conjunction with OLEX2 software.<sup>4-6</sup> None of the crystals demonstrated decay by X-ray radiation over the course of the experiment. Hydrogen atoms were placed in ideal positions and refined using a riding model for all structures. In **1**, carbon atoms in their respective phenyl groups were restrained to be coplanar and C–C bond lengths were restrained to be within a standard error of 0.01 Å. In one of the methanol solvent molecules, disordered molecules freely modeling two positions yielded occupancies of 0.60(6) and 0.30(6). In one of the methanol solvent molecules, a disordered carbon freely modeling two positions yielded an occupancy of 0.62(4) and 0.38(4). In two methanol solvent molecules, disordered molecules were modeled with fixed occupancies of 0.50 and 0.50. In **4**, four 1,3-diaminopropane ligands were freely modeled over two positions yielding occupancies of 0.54(7) and 0.46(7), 0.51(6) and 0.49(6), 0.57(2) and 0.43(2), 0.66(4) and 0.34(4). In one ethanol solvent molecule, the disorder over two positions yielded occupancies 0.51(3) and 0.49(3). In two water solvent molecules, disordered molecules were modeled with fixed occupancies of 0.50 and 0.50. And finally, in one chloride counterion, disorder modeled over two positions yielded occupancies of 0.580(11) and 0.420(11). In **5-RR**, two disordered water molecules free modeling two positions yielded occupancies of 0.687(20) and 0.313(9) for each. A disordered chloride counterion freely modeling two positions yielded occupancies of 0.684(9) and 0.316(9). Crystallographic information files for **1**, **4**, **5-SS**, and **5-RR** are available in the CSD at accession numbers 2041467-2041470.

**Electron Paramagnetic Resonance.** EPR spectra collected herein were simulated using Easyspin<sup>7</sup> with the function pepper (frozen solution and solid) and were refined using the function esfit or simulations of the experimental data. All samples were prepared at atmospheric conditions as 30 mM aqueous solutions in ethylene glycol (1:1 v/v) the same day that the measurements took place. X-band CW EPR data were collected for all compounds on a Bruker ESR-300 spectrometer and was carried out at 80 K using a liquid nitrogen cooled cryostat or at 77K in a liquid nitrogen filled quartz finger dewar.

L-band EPR spectra were performed on two different instruments. L-band CW EPR was performed on compounds **1**, **2**, **3**, **4**, and **5** on a low-frequency spectrometer station assembled at the National Biomedical EPR Center at the Medical College of Wisconsin (Milwaukee, WI, USA).

The station incorporates an in-house-built L-band (1–2 GHz) bridge, Varian V-7200 Electromagnet, Varian V-7700 Magnet Power Supply, and Bruker BH-15 Magnetic Field Controller. The 100 KHz field modulation and signal phase-sensitive detection were provided by a Varian E-109 System EPR console. EPR signals from the phase-sensitive detector were recorded on a PC with Windows 7 running a custom LabVIEW program. The program also controlled the BH-15 Field Controller and performed multiple-scan signal averaging, when needed. The L-band bridge in the spectrometer utilizes a low-phase-noise, mechanically and electronically tunable fundamental transistor oscillator capable of 50 mW power output to the sample resonator port at 0 dB main power attenuator setting. A loop-gap resonator was used to collect samples. The oscillator microwave frequency was locked to the sample resonator frequency by a 70 KHz automatic frequency control system in the bridge, operating through the electronic tuning port of the oscillator. A low-noise amplifier in the microwave signal receiver prior to signal mixing improved the overall bridge sensitivity. L-band CW EPR analyses were also performed on **5-SS** on a locally-constructed 1-2 GHz spectrometer described in Quine et al., 1996.<sup>8</sup> Major changes include collecting the signal in a Bruker Specjet digitizer, controlling the magnetic field with a BH15 field controller, and replacing a Varian power supply with a Bruker EMX080 power supply. The resonator was a Bruker ER4118L-MS5 splitting module mounted on an ER4118SPT Flexline probe head support. 4 or 5 mm diameter sample tubes can be used. The Flexline mounted resonator was in a Bruker/Oxford CF935 continuous flow cryostat, through which liquid nitrogen was passed to achieve the 80K operating temperature. When sample size is kept constant and the frequency is lowered from X-band to L-band, sensitivity decreases by about a factor of 50 if the sample size and resonator size are kept constant.<sup>9</sup> Consequently, signal-to-noise at 1 GHz using standard 4 mm o.d. quartz sample tubes is very low relative to normal X-band CW EPR experience. The signal-to-noise specification for this resonator, if used with a Bruker bridge, was 300:1 for Bruker strong (not weak) pitch, using 6 G modulation amplitude.

**Explanations of EPR Simulations.** L-band (1.360 GHz) EPR spectra were simulated with the EasySpin software package.<sup>7</sup> Axial  $g$ -values and a single zero-field splitting term ( $D$ ) were modeled as the spin Hamiltonian parameters. Broadening was modeled as a distribution of  $g$ -values by the method of explicit averaging over distributions, as described in the EasySpin documentation. With this method, two distributions of  $g_{xy}$ - and  $g_z$ -values were defined along

gaussian distributions, each defined by a mean  $g$ -value (Table S11), the bounds of the distribution, and full-width at half-maximum (Table S11). For each  $g$ -value, there is a corresponding weight to where it resides on the gaussian curve, with the highest weights corresponding to  $g$ -values close to the mean, and the lowest corresponding to those in the peripheries. An EPR spectrum is simulated with each combination of  $g_{xy}$ - and  $g_z$ -values, then multiplied by their corresponding weights. Each spectrum is then summed to give the final EPR spectrum. The LWPP (Table S11) broadening term was included to give each simulation a “natural” linewidth as to avoid simulating an exuberant amount of EPR spectra per complex. A single  $D$ -value was used for each complex in the final simulations; however, incorporation of an  $E$ -value was attempted, but yielded no improvement in the spectral simulations and drastically increased the computational time required. The standard signal selection rule threshold limit of  $1 \times 10^{-4}$  was used when simulating the reported EPR spectra.

We note that the method described above is unprecedented and rather unusual in the way it models the EPR line shapes of the complexes described herein. We had attempted more conventional methods of modeling broadening, including the built-in functions modeling isotropic broadening,  $g$ -strain and  $D/E$ -strain, and a similar method as described above modeling a distribution of  $D$  and  $E$  values. However, none of these methods produced simulations that matched the experimental spectra as closely as modeling a distribution of  $g$ -values.

Finally, for discussions of  $\text{Cr}^{3+}$  CW line shapes and relaxation, it is important that there are 3 transitions,  $^{3/2} \rightarrow ^{1/2}$ ,  $^{1/2} \rightarrow ^{-1/2}$ , and  $^{-1/2} \rightarrow ^{-3/2}$  that arise from the zero-field splitting. These transitions may have different relaxation times and therefore different linewidths. The  $g$  value is usually about 1.98. The  $D$  and  $E$  values that characterize zero-field splittings (ZFS) caused by spin-orbit couplings vary over a wide range in ways that are difficult to relate to the structure of the ligands. Consequently, simulating EPR spectra of  $\text{Cr}^{3+}$  complexes is inexact at best. The simulations presented in the present paper, using distributions in  $g_x$  and  $g_y$ , although matching the broad experimental spectra reasonably well, do not have clear physical meaning. This type distribution has not been found in prior literature. More commonly broad lines for Cr(III) have been simulated with distributions in the ZFS parameters, which are known to be highly sensitive to local environment.<sup>10–13</sup> The comparison with the spectra in ref. 49 the main manuscript of high-spin Co(II) does invoke large  $g$  anisotropy, which is common of high-spin Co(II) but not for Cr(III), but appears amplified in the current manuscript owing to the use of the low frequency.

Future multifrequency studies will probably be necessary to sort out the *D* and *E* ranges consistent with the L-band spectra.

**Other Physical Measurements.** Elemental analyses were performed by Roberson Microlit Laboratories (Ledgewood, New Jersey, USA). Infrared spectra were recorded on a Nicolet 6700 FTIR spectrometer using a diamond window ATR. Electronic absorption spectra of all complexes were recorded on aqueous with a Hewlett-Packard 8453 spectrophotometer using standard quartz cuvettes with a 1 cm path length. Mass spectral analyses were performed on an Agilent 6224 Accurate Mass TOF LC/MS in positive ion mode using direct injection. Peak assignment was on the basis of *m/z*, interpeak spacing, and isotopic distribution. Emission spectra were obtained on an Edinburgh FS5 Spectrofluorometer using a quartz cuvette with a 1 cm path length in a temperature controlled sample holder. Samples were prepared as 30 mM solutions in water and held at 20 °C. Steady state emission spectra were obtained by exciting each sample at 460 nm with a 6.0 nm slit width and collecting from 480—800 nm. Spectra were averaged over three scans with a 0.5 s integration time. Time resolved emission spectra were obtained over a 500 ns time range with a repetition frequency of 2 MHz. Samples were excited with a 450 nm EPL picosecond pulsed diode laser and collected at 670 nm with a bandwidth of 20 nm.

### Computational Details

**Cluster Global Optimization Details:** The structures of Cr(III) complexes **1**, **2**, **4**, **5**, each micro-solvated by 20 water molecules were determined using NWPEsSe,<sup>14</sup> a global optimization method based on the artificial bee colony algorithm.<sup>15,16</sup> For each system, the search included 500 structures with the xTB method, and the lowest 10 structures were further optimized at the TPSSh+D3/def2-TZVP level of theory. The most stable one was taken as the minimum. These most-stable clusters are shown in Figure S11.

Using the most stable structures determined from the global optimization above, four simulation boxes were set up with the following contents. For **1**, the box contained [Cr(*RR*-dphen)<sub>3</sub>]<sup>3+</sup>, 3 × Cl<sup>-</sup> anions, and 300 H<sub>2</sub>O molecules. For **2**, the box contained [Cr(en)<sub>3</sub>]<sup>3+</sup>, 3 × Cl<sup>-</sup> anions, and 150 H<sub>2</sub>O molecules. For **4**, the box contained [Cr(tn)<sub>3</sub>]<sup>3+</sup>, 3 × Cl<sup>-</sup> anions, and 180 H<sub>2</sub>O molecules. For **5**, the box contained [Cr(*trans*-chxn)<sub>3</sub>]<sup>3+</sup>, 3 × Cl<sup>-</sup> anions, and 180 H<sub>2</sub>O molecules. The boxes were first equilibrated under *P* = 1 atm and *T* = 300 K. The OPLS force fields<sup>17</sup> were

used as implemented in the GROMACS program.<sup>18</sup> Following the NPT simulation, the cell parameter were fixed at 21.8 Å, (complex **1**), 17.1 Å (complex **2**), 18.1 Å, (complex **4**), and 19.2 Å, (complex **5**) and the four systems were equilibrated and allowed to run for about 10 ns in the NVT ensemble. These trajectories were used for the analysis of the results.

**Table S1.** Crystallographic information for the structural refinement of **1**.

Empirical formula	C <sub>96</sub> H <sub>138</sub> Cl <sub>6</sub> Cr <sub>2</sub> N <sub>12</sub> O <sub>9</sub> S <sub>2</sub>
Formula weight	1985.00 g/mol
Temperature	100.02 K
Crystal system	Monoclinic
Space group	P2 <sub>1</sub>
<i>a</i>	12.3901(5) Å
<i>b</i>	19.3151(8) Å
<i>c</i>	24.4122(11) Å
$\alpha$	90°
$\beta$	104.287(2)°
$\gamma$	90°
Volume	5661.5(4) Å <sup>3</sup>
<i>Z</i>	2
$\rho_{\text{calc}}$	1.164 g cm <sup>-3</sup>
$\mu$	0.424 mm <sup>-1</sup>
F(000)	2104.0
Crystal color	Orange
Crystal size	0.224 × 0.151 × 0.086 mm <sup>3</sup>
Radiation	MoK $\alpha$ ( $\lambda$ = 0.71073 Å)
2 $\theta$ range for data collection	1.722 to 49.42°
Index ranges	-14 ≤ <i>h</i> ≤ 14, -22 ≤ <i>k</i> ≤ 22, -28 ≤ <i>l</i> ≤ 28
Reflections collected	151263
Independent collections	19288 [ <i>R</i> <sub>int</sub> = 0.0591, <i>R</i> <sub>sigma</sub> = 0.0339]
Data/restraints/parameters	19288/762/1158
Goodness-of-fit on <i>F</i> <sup>2</sup>	1.040
Final <i>R</i> indexes [ <i>I</i> ≥ 2 $\sigma$ ( <i>I</i> )]	<i>R</i> <sub>1</sub> = 0.0853, <i>wR</i> <sub>2</sub> = 0.2412
Final <i>R</i> indexes [all data]	<i>R</i> <sub>1</sub> = 0.1009, <i>wR</i> <sub>2</sub> = 0.2622
Largest diff. peak/hole	1.45/-1.19 e Å <sup>-3</sup>
Flack parameter	0.044(6)

**Table S2.** Crystallographic information for the structural refinement of **4**.

Empirical formula	C <sub>20</sub> H <sub>74</sub> Cl <sub>6</sub> Cr <sub>2</sub> N <sub>12</sub> O <sub>5</sub>
Formula weight	879.61 g/mol
Temperature	154.01 K
Crystal system	Monoclinic
Space group	Cc
<i>a</i>	28.4948(19) Å
<i>b</i>	12.0595(7) Å
<i>c</i>	14.7903(8) Å
$\alpha$	90°
$\beta$	121.059(3)°
$\gamma$	90°
Volume	4353.8(5) Å <sup>3</sup>
<i>Z</i>	4
$\rho_{\text{calc}}$	1.342 g cm <sup>-3</sup>
$\mu$	0.910 mm <sup>-1</sup>
F(000)	1878.5
Crystal color	Orange
Crystal size	0.253 × 0.136 × 0.103 mm <sup>3</sup>
Radiation	MoK $\alpha$ ( $\lambda$ = 0.71073 Å)
2 $\theta$ range for data collection	3.214 to 64.258°
Index ranges	-42 ≤ <i>h</i> ≤ 42, -18 ≤ <i>k</i> ≤ 18, -22 ≤ <i>l</i> ≤ 22
Reflections collected	69980
Independent collections	12060 [ <i>R</i> <sub>int</sub> = 0.0499, <i>R</i> <sub>sigma</sub> = 0.0382]
Data/restraints/parameters	12060/9/394
Goodness-of-fit on <i>F</i> <sup>2</sup>	1.116
Final <i>R</i> indexes [ <i>I</i> ≥ 2 $\sigma$ ( <i>I</i> )]	<i>R</i> <sub>1</sub> = 0.0667, <i>wR</i> <sub>2</sub> = 0.1883
Final <i>R</i> indexes [all data]	<i>R</i> <sub>1</sub> = 0.0878, <i>wR</i> <sub>2</sub> = 0.2117
Largest diff. peak/hole	1.53/-1.78 e Å <sup>-3</sup>
Flack parameter	0.021(7)

**Table S3.** Crystallographic information for the structural refinement of **5-SS**.

---

Empirical formula	C <sub>18</sub> H <sub>52</sub> Cl <sub>3</sub> CrN <sub>6</sub> O <sub>5</sub>
Formula weight	591.01 g/mol
Temperature	99.99 K
Crystal system	Hexagonal
Space group	P6 <sub>1</sub>
<i>a</i>	12.2492(5) Å
<i>b</i>	12.2492(5) Å
<i>c</i>	33.5991(16) Å
$\alpha$	90°
$\beta$	90°
$\gamma$	120°
Volume	4365.9(4) Å <sup>3</sup>
<i>Z</i>	6
$\rho_{\text{calc}}$	1.349 g cm <sup>-3</sup>
$\mu$	0.705 mm <sup>-1</sup>
F(000)	1902.0
Crystal color	Orange
Crystal size	0.123 × 0.088 × 0.086 mm <sup>3</sup>
Radiation	MoK $\alpha$ ( $\lambda$ = 0.71073 Å)
2 $\theta$ range for data collection	3.84 to 50.024°
Index ranges	-14 ≤ <i>h</i> ≤ 13, -14 ≤ <i>k</i> ≤ 13, -39 ≤ <i>l</i> ≤ 39
Reflections collected	19578
Independent collections	5157 [ <i>R</i> <sub>int</sub> = 0.0509, <i>R</i> <sub>sigma</sub> = 0.0504]
Data/restraints/parameters	5157/3/313
Goodness-of-fit on <i>F</i> <sup>2</sup>	1.097
Final <i>R</i> indexes [ <i>I</i> ≥ 2 $\sigma$ ( <i>I</i> )]	<i>R</i> <sub>1</sub> = 0.0560, <i>wR</i> <sub>2</sub> = 0.1362
Final <i>R</i> indexes [all data]	<i>R</i> <sub>1</sub> = 0.0650, <i>wR</i> <sub>2</sub> = 0.1472
Largest diff. peak/hole	1.84/-0.65 e Å <sup>-3</sup>
Flack parameter	0.031(13)

**Table S4.** Crystallographic information for the structural refinement of **5-RR**.

---

Empirical formula	C <sub>18</sub> H <sub>52</sub> Cl <sub>3</sub> CrN <sub>6</sub> O <sub>5</sub>
Formula weight	591.01 g/mol
Temperature	100.0 K
Crystal system	Hexagonal
Space group	P6 <sub>5</sub>
<i>a</i>	12.2603(6) Å
<i>b</i>	12.2603(6) Å
<i>c</i>	33.2599(16) Å
$\alpha$	90°
$\beta$	90°
$\gamma$	120°
Volume	4329.7(5) Å <sup>3</sup>
<i>Z</i>	6
$\rho_{\text{calc}}$	1.360 g cm <sup>-3</sup>
$\mu$	0.711 mm <sup>-1</sup>
F(000)	1902.0
Crystal color	Orange
Crystal size	0.121 × 0.104 × 0.079 mm <sup>3</sup>
Radiation	MoK $\alpha$ ( $\lambda$ = 0.71073 Å)
2 $\theta$ range for data collection	4.026 to 52.73°
Index ranges	-15 ≤ <i>h</i> ≤ 15, -15 ≤ <i>k</i> ≤ 15, -41 ≤ <i>l</i> ≤ 41
Reflections collected	171415
Independent collections	5914 [ <i>R</i> <sub>int</sub> = 0.0669, <i>R</i> <sub>sigma</sub> = 0.0184]
Data/restraints/parameters	5914/112/330
Goodness-of-fit on <i>F</i> <sup>2</sup>	1.081
Final <i>R</i> indexes [ <i>I</i> ≥ 2 $\sigma$ ( <i>I</i> )]	<i>R</i> <sub>1</sub> = 0.0561, <i>wR</i> <sub>2</sub> = 0.1251
Final <i>R</i> indexes [all data]	<i>R</i> <sub>1</sub> = 0.0608, <i>wR</i> <sub>2</sub> = 0.1288
Largest diff. peak/hole	1.09/-0.88 e Å <sup>-3</sup>
Flack parameter	0.020(6)

**Table S5.** Selected inner coordination sphere bond lengths and angles of **1**.

Atoms	Length (Å)	Atoms	Angle (°)
Cr01–N00C	2.087(7)	N00E–Cr01–N00G	82.0(3)
Cr01–N00E	2.078(7)	N00F–Cr01–N00H	82.3(3)
Cr01–N00F	2.050(8)	N00I–Cr01–N00C	82.0(3)
Cr01–N00G	2.078(7)	N00F–Cr01–N00E	171.0(3)
Cr01–N00H	2.073(7)	N00G–Cr01–N00C	169.8(3)
Cr01–N00I	2.080(7)	N00H–Cr01–N00I	169.6(3)
Cr02–N00K	2.083(8)	N00N–Cr02–N00V	81.6(3)
Cr02–N00N	2.070(8)	N00S–Cr02–N00K	80.8(3)
Cr02–N00P	2.097(7)	N01D–Cr02–N00P	81.0(3)
Cr02–N00S	2.083(9)	N00N–Cr02–N00P	171.0(3)
Cr02–N00V	2.075(8)	N00V–Cr02–N00K	172.4(3)
Cr02–N01D	2.068(9)	N01D–Cr02–N00S	173.7(3)

**Table S6.** Selected inner coordination sphere bond lengths and angles of **4**.

Atoms	Length (Å)	Atoms	Angle (°)
Cr01–N009	2.098(7)	N00Q–Cr01–N00K	91.2(6)
Cr01–N00C	2.096(7)	N00R–Cr01–N00K	87.6(5)
Cr01–N00I	2.078(7)	N1–Cr01–N009	89.0(5)
Cr01–N00J	2.138(16)	N00I–Cr01–N00J	85.6(5)
Cr01–N00K	2.089(7)	N00I–Cr01–N00C	90.5(3)
Cr01–N00Q	2.045(17)	N00C–Cr01–N00R	173.8(6)
Cr01–N1	2.078(17)	N00I–Cr01–N009	176.8(3)
Cr01–N00R	2.144(14)	N00K–Cr01–N00J	175.6(6)
Cr02–N00D	2.35(3)	N00Q–Cr01–N00C	174.8(8)
Cr02–N00E	1.930(17)	N1–Cr01–N00K	174.7(7)
Cr02–N00H	2.207(17)	N2AA–Cr02–N00V	94.6(6)
Cr02–N00U	2.18(2)	N00D–Cr02–N00U	80.6(9)
Cr02–N0AA	2.195(15)	N4AA–Cr02–N3AA	90.4(4)
Cr02–N1AA	2.029(13)	N0AA–Cr02–N1AA	90.8(6)
Cr02–N00V	2.074(13)	N00E–Cr02–N00H	92.2(7)
Cr02–N2AA	1.971(17)	N00E–Cr02–N00D	173.2(8)
Cr02–N3AA	2.117(8)	N1AA–Cr02–N4AA	173.1(5)
Cr02–N4AA	2.105(10)	N2AA–Cr02–N0AA	172.4(6)
		N3AA–Cr02–N00U	169.1(9)
		N4AA–Cr02–N00H	172.4(6)
		N00V–Cr02–N3AA	175.9(5)

**Table S7.** Selected inner coordination sphere bond lengths and angles of **5-RR**.

Atoms	Length (Å)	Atoms	Angle (°)
Cr01–N005	2.079(5)	N007–Cr01–N005	82.57(19)
Cr01–N006	2.083(5)	N008–Cr01–N006	82.14(19)
Cr01–N007	2.078(5)	N00A–Cr01–N00B	82.2(2)
Cr01–N008	2.081(5)	N005–Cr01–N006	170.96(19)
Cr01–N00A	2.065(5)	N00A–Cr01–N007	170.2(2)
Cr01–N00B	2.074(5)	N00B–Cr01–N008	172.5(2)

**Table S8.** Selected inner coordination sphere bond lengths and angles of **5-SS**.

Atoms	Length (Å)	Atoms	Angle (°)
Cr01–N005	2.088(6)	N006–Cr01–N007	81.7(2)
Cr01–N006	2.076(6)	N008–Cr01–N00A	82.4(2)
Cr01–N007	2.084(6)	N009–Cr01–N005	82.4(2)
Cr01–N008	2.080(6)	N006–Cr01–N005	170.8(2)
Cr01–N009	2.085(7)	N007–Cr01–N00A	172.2(2)
Cr01–N00A	2.086(6)	N008–Cr01–N009	170.2(2)

**Table S9.** Continuous-shape-measurement (CSM) (SHAPE 2.0 software)<sup>19,20</sup> results for **1**, **2**, **4**, **5**, **5-SS**, **5-RR**.

Complex	SHAPE analysis octahedral	SHAPE analysis trigonal prismatic
<b>1</b>	0.731	12.69
<b>2</b>	0.616	13.43
<b>4</b>	0.064	15.73
<b>5</b>	0.510	13.79
<b>5-SS</b>	0.661	12.54
<b>5-RR</b>	0.636	12.55

**Table S10.** Emission lifetimes for **1-5** obtained through bi-exponential decay (**2-5**, **5-SS**, and **5-RR**) or tri-exponential decay (**1**) fits.

Complex	$\tau_1$ (ns)	$\tau_2$ (ns)	$\tau_3$ (ns)
<b>1</b>	0.45 ± 0.033	37.9 ± 4.7	1884 ± 66
<b>2</b>	1.40 ± 0.049	1800 ± 37	-
<b>3</b>	0.99 ± 0.054	1830 ± 32	-
<b>4</b>	0.48 ± 0.062	1950 ± 29	-
<b>5</b>	0.97 ± 0.059	1910 ± 34	-
<b>5-SS</b>	0.72 ± 0.034	1550 ± 23	-
<b>5-RR</b>	0.58 ± 0.048	1590 ± 21	-

**Table S11.** Spin Hamiltonian parameters for **1-5** in ethylene glycol-water solutions (50:50 v/v) collected at 112 K by CW L-band EPR. The standard errors for these parameters were not available from the simulating process.

	<b>1</b>	<b>2</b>	<b>3</b>	<b>4</b>	<b>5</b>	<b>5-SS</b>
$g_{x,y}$	1.995	1.985	1.985	2.300	2.300	2.300
$g_z$	1.955	1.960	1.970	1.990	2.000	2.000
$D$ (cm <sup>-1</sup> )	0.11	0.10	0.093	0.097	0.097	0.097
$g_{xy}$ FWHM	0.60	0.80	1.12	3.80	4.10	4.10
$g_z$ FWHM	0.01	0.10	0.80	0.38	0.40	0.40
LWPP	2.2	3.2	3.2	3.9	3.9	3.9

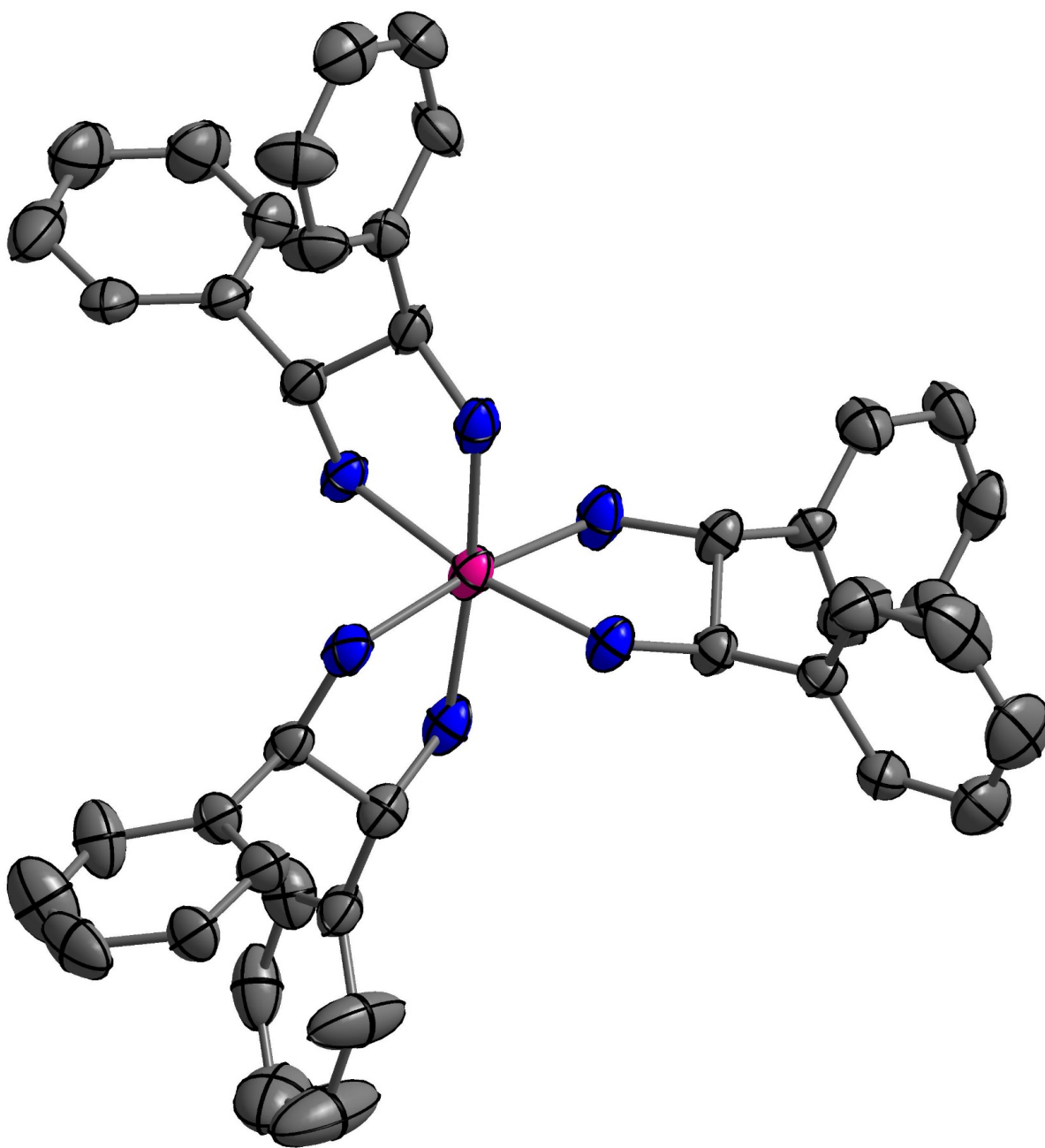


**Figure S1.** Thermal ellipsoid plot of **1** drawn at the 50% probability level. Hydrogen atoms, counterions, and solvent molecules were removed for clarity. Pink, blue, and grey ellipsoids correspond to chromium, nitrogen, and carbon, respectively.

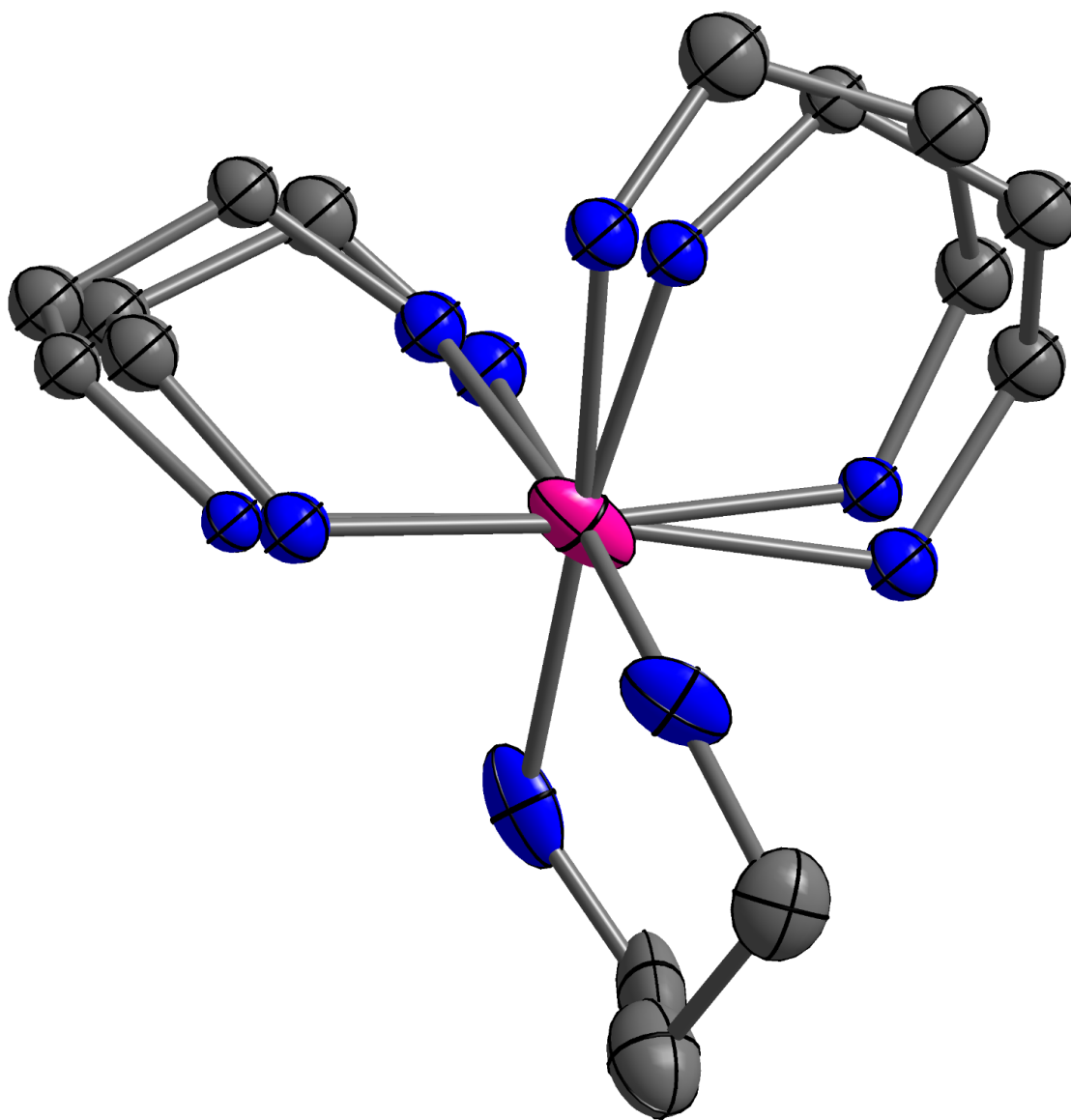


**Figure S2.** Thermal ellipsoid plot of **4** drawn at the 50% probability level. Disorder is illustrated for two of the 1,3-propanediamine arms. Hydrogen atoms, counterions, and solvent molecules were removed for clarity. Pink, blue, and grey ellipsoids correspond to chromium, nitrogen, and carbon atoms, respectively.

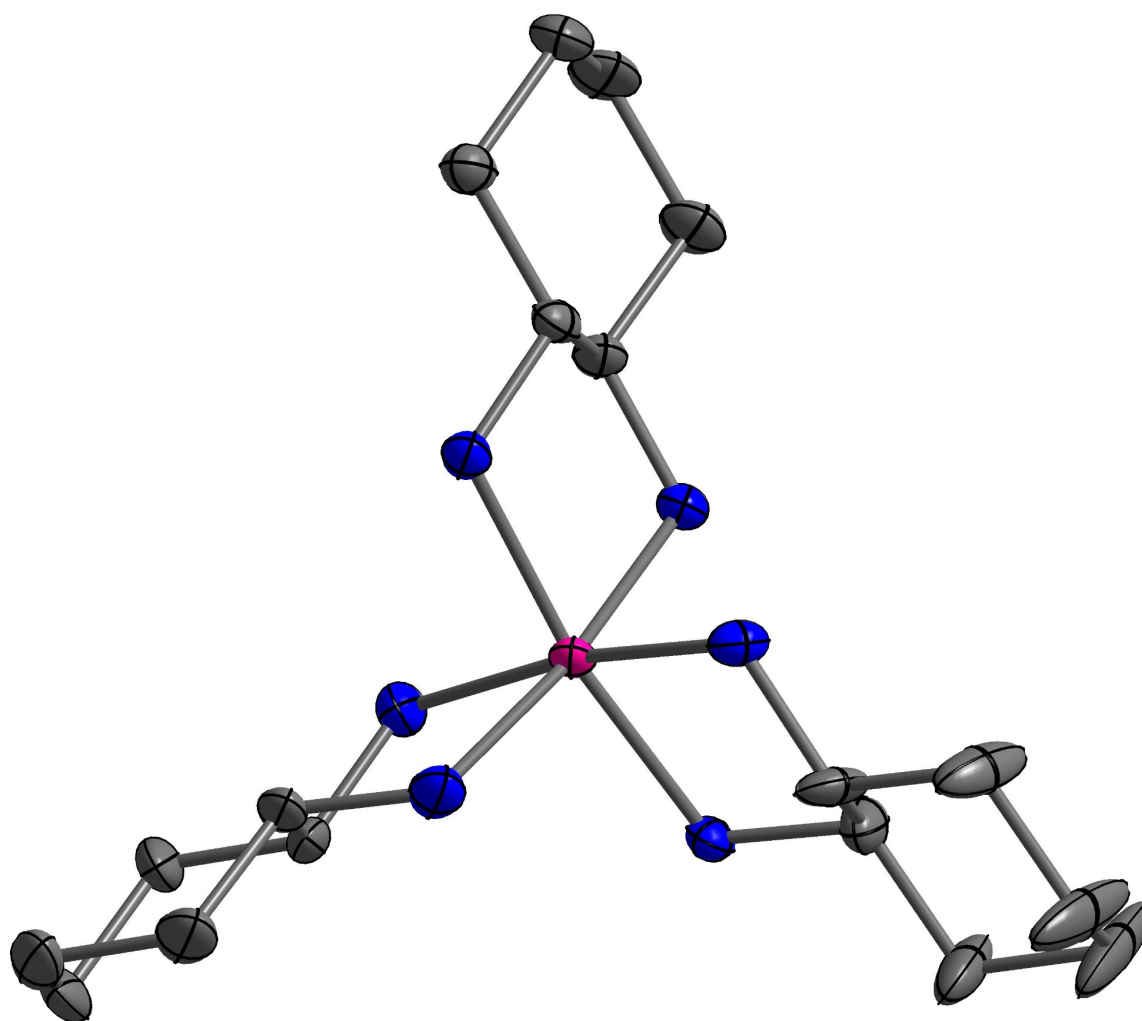


**Figure S3.** Thermal ellipsoid plot of **5-RR** drawn at the 50% probability level. Hydrogen atoms, counterions, and solvent molecules were removed for clarity. Pink, blue, and grey ellipsoids correspond to chromium, nitrogen, and carbon atoms, respectively.

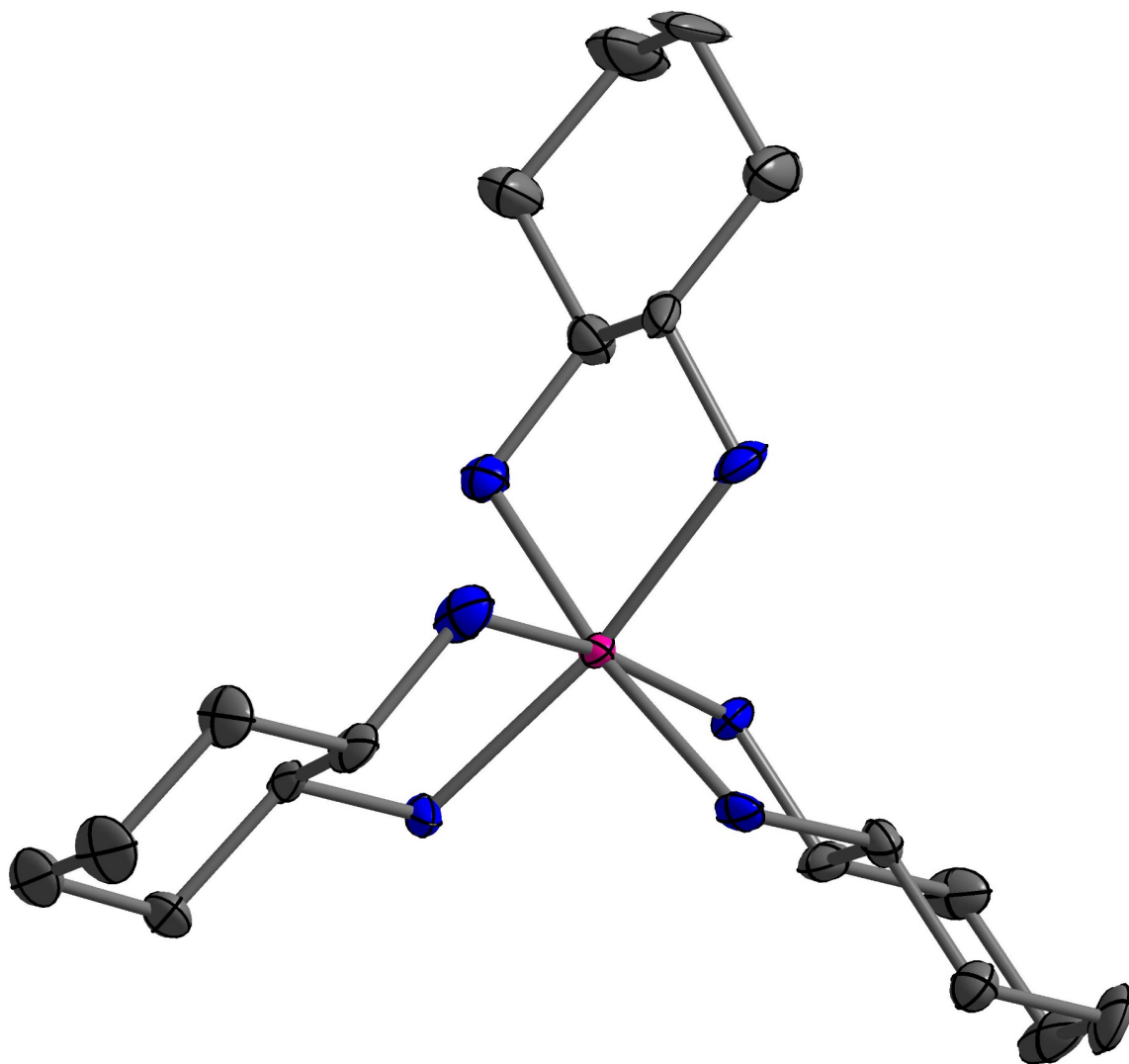


**Figure S4.** Thermal ellipsoid plot of **5-SS** drawn at the 70% probability level. Hydrogen atoms, counterions, and solvent molecules were removed for clarity. Pink, blue, and grey ellipsoids correspond to chromium, nitrogen, and carbon atoms, respectively.

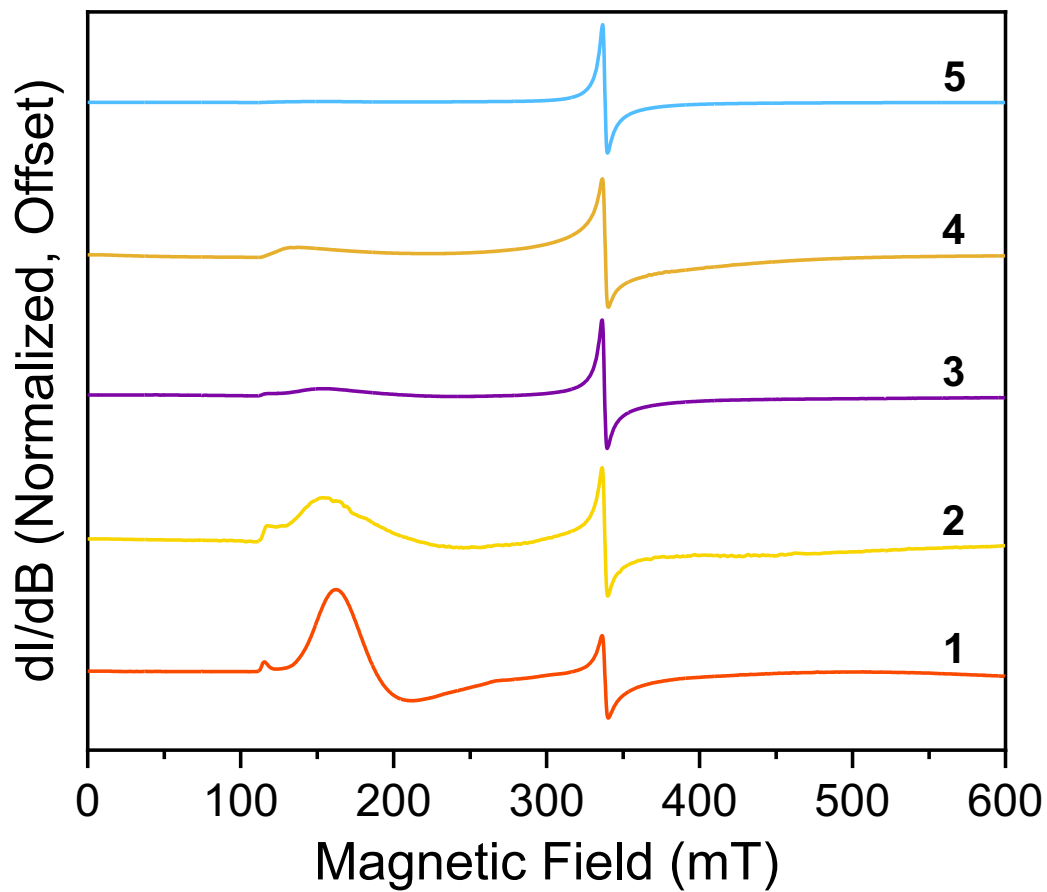


**Figure S5.** Continuous-wave X-band EPR spectra of **1-5** in ethylene glycol-water solutions (50:50 v/v) collected at 77 K.

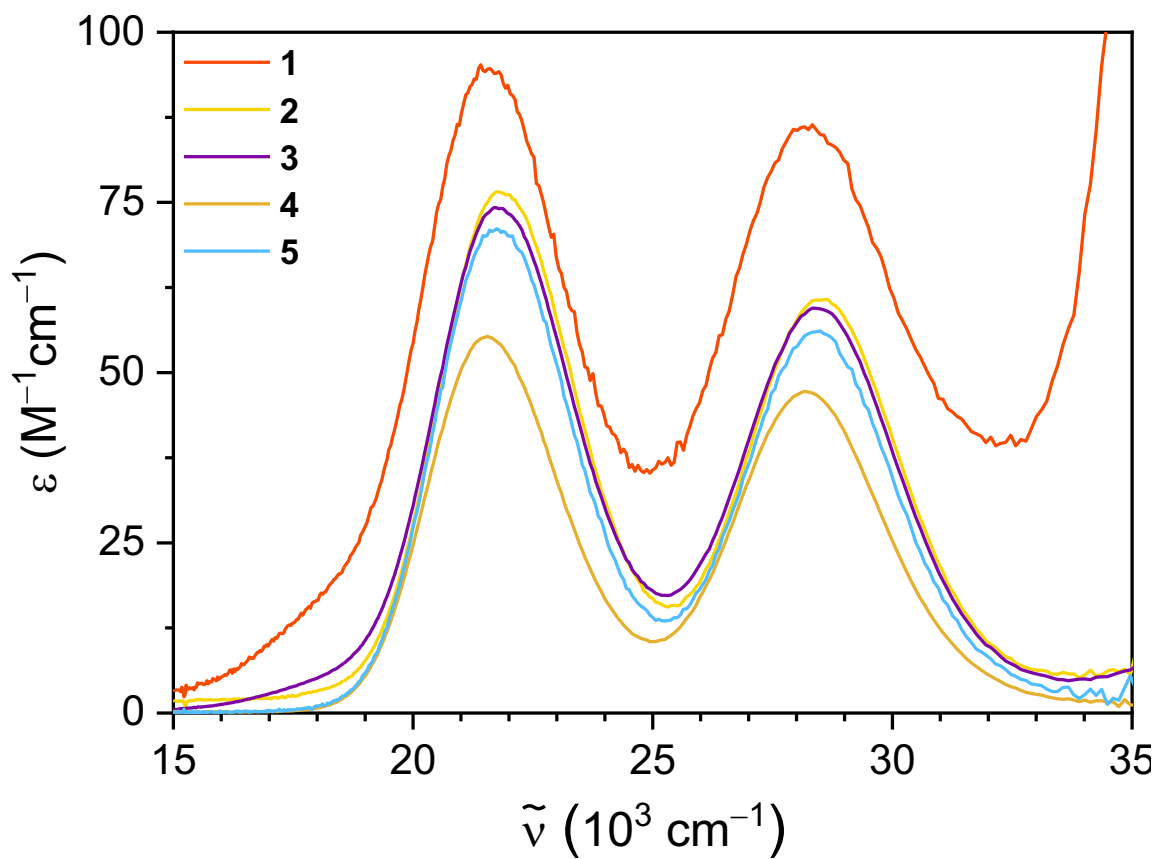


**Figure S6.** Electronic absorption spectroscopy data for complexes **1-5**. Solutions were prepared at ca. 1, 5, and 10 mM in deionized H<sub>2</sub>O and spectra were collected at room temperature.

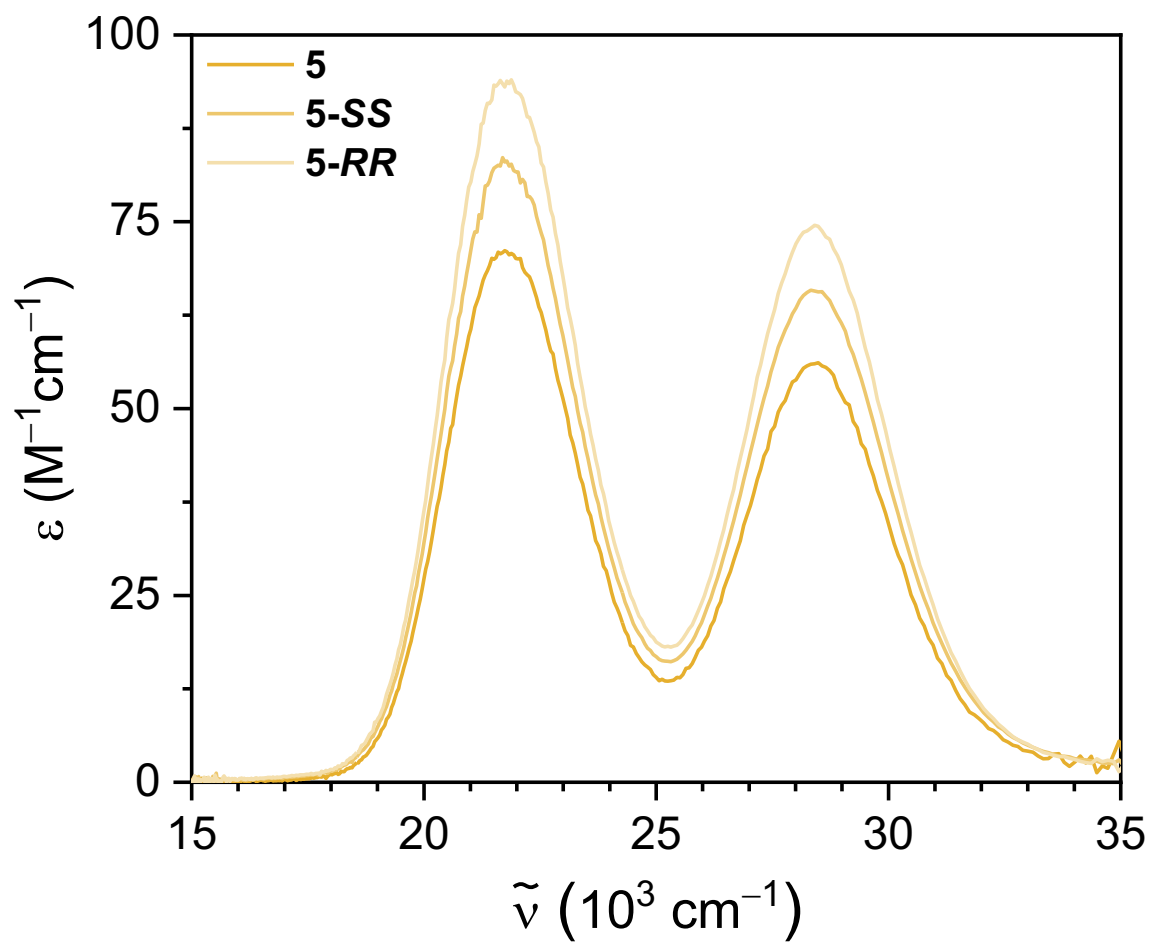


**Figure S7.** Electronic absorption spectroscopy data for complexes **5**, **5-SS**, and **5-RR**. Solutions were prepared at ca. 1, 5, and 10 mM in deionized  $\text{H}_2\text{O}$  and spectra were collected at room temperature.

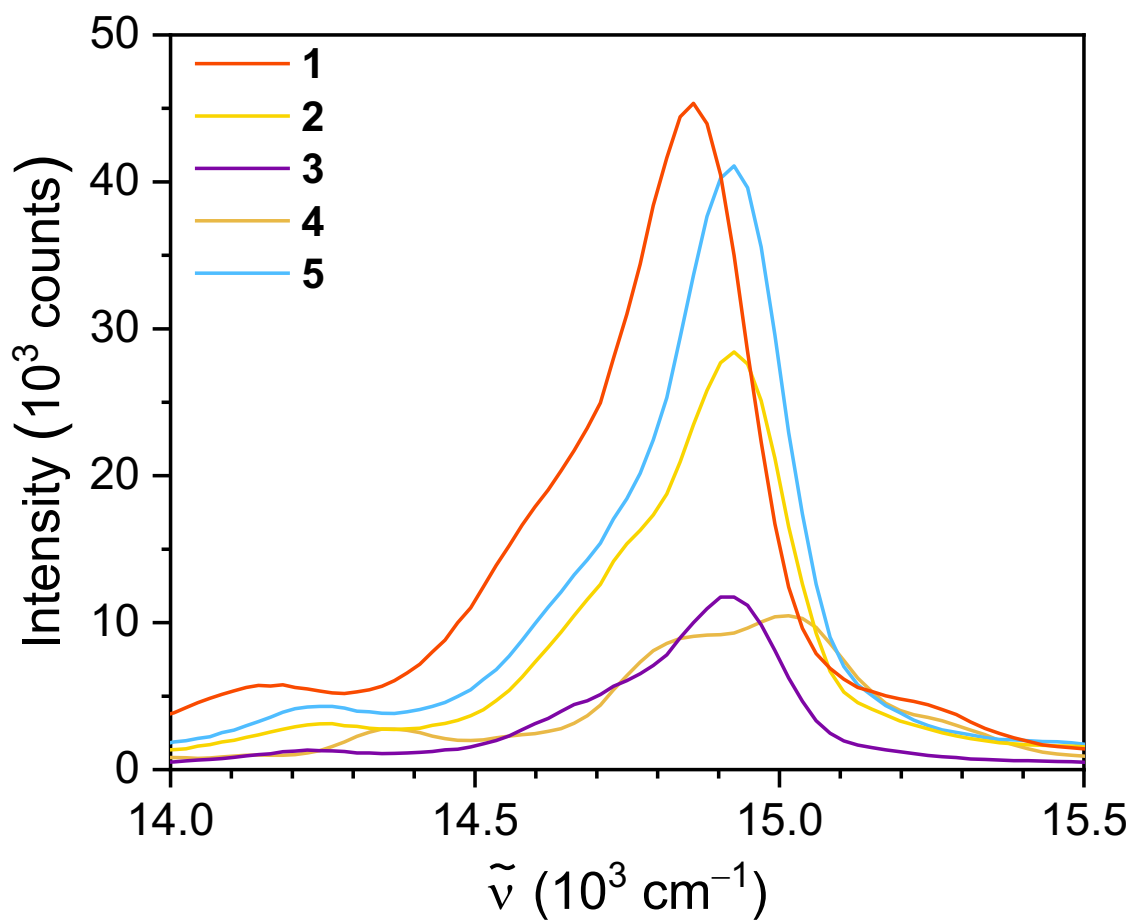


**Figure S8.** Steady-state emission spectroscopy data for **1-5**. Solutions were prepared at ca. 30 mM in deionized H<sub>2</sub>O and spectra were collected at 20 °C.

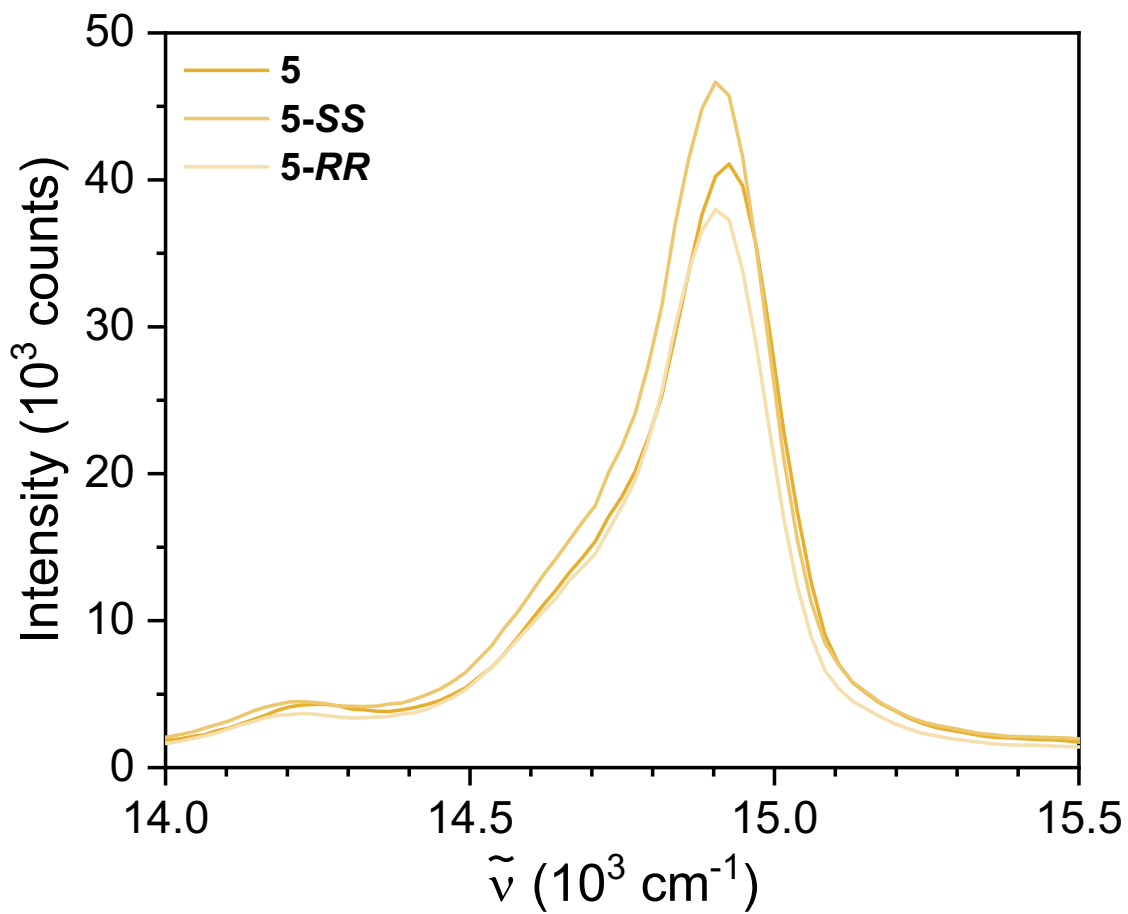


**Figure S9.** Steady-state emission spectroscopy data for **5**, **5-SS**, and **5-RR**. Solutions were prepared at ca. 30 mM in deionized H<sub>2</sub>O and spectra were collected at 20 °C.

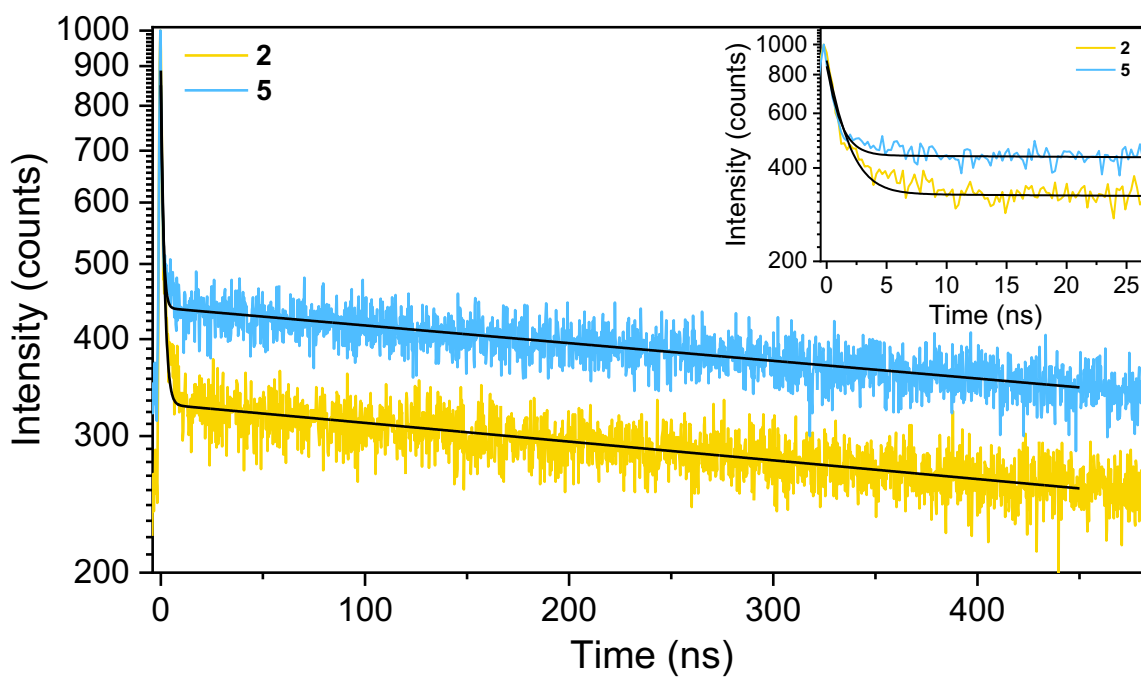


**Figure S10.** Time-resolved emission spectra for **2** and **5**. The solutions were prepared at ca. 30 mM in deionized H<sub>2</sub>O and spectra were collected at 20 °C.

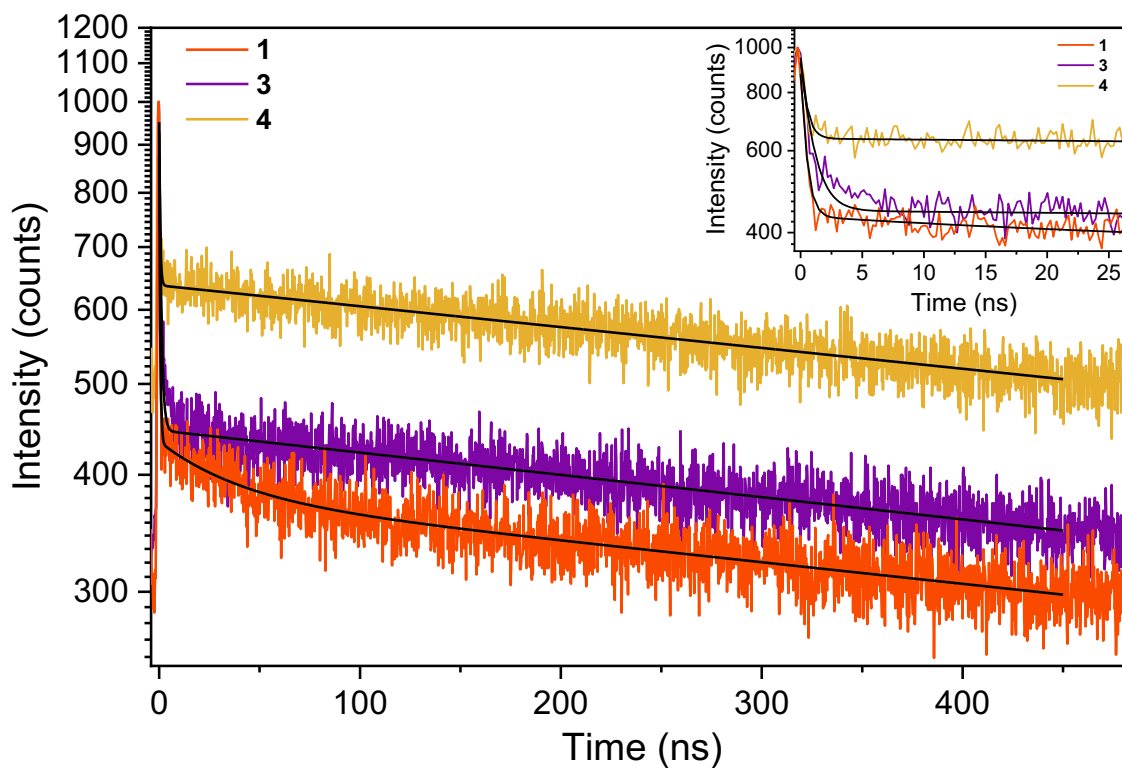


**Figure S11.** Time-resolved emission spectra for **1**, **3** and **4**. The solutions were prepared at ca. 30 mM in deionized H<sub>2</sub>O and spectra were collected at 20 °C.

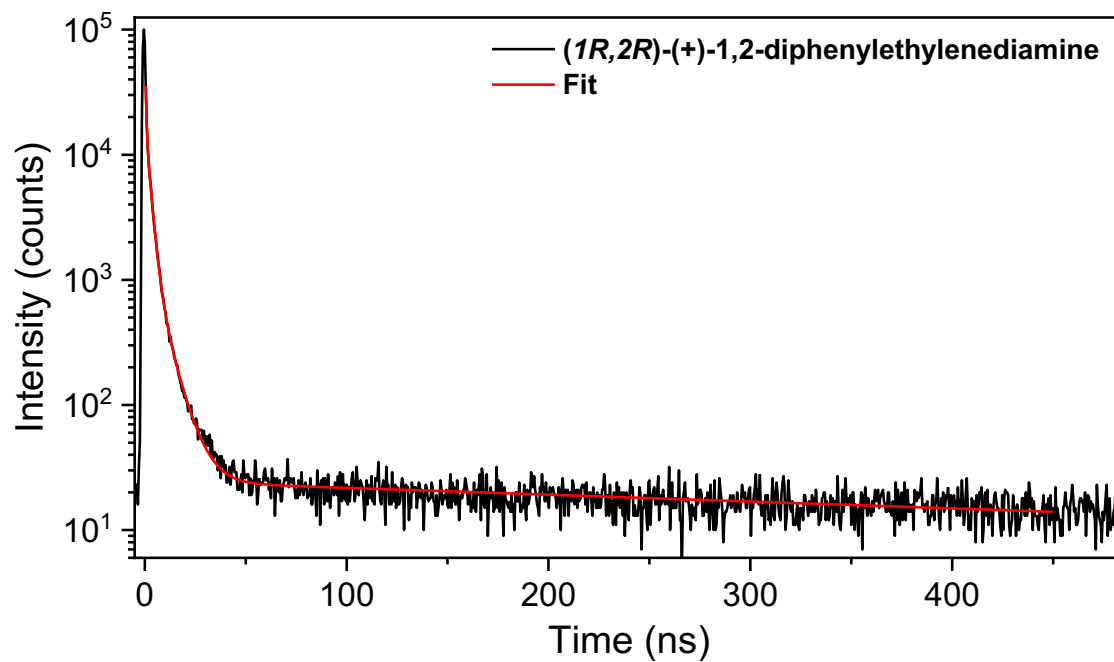


**Figure S12.** Time-resolved emission spectra for (1R,2R)-(+)-1,2-diphenylethylenediamine. The solution was prepared at ca. 30 mM in deionized H<sub>2</sub>O and spectra were collected at 20 °C.

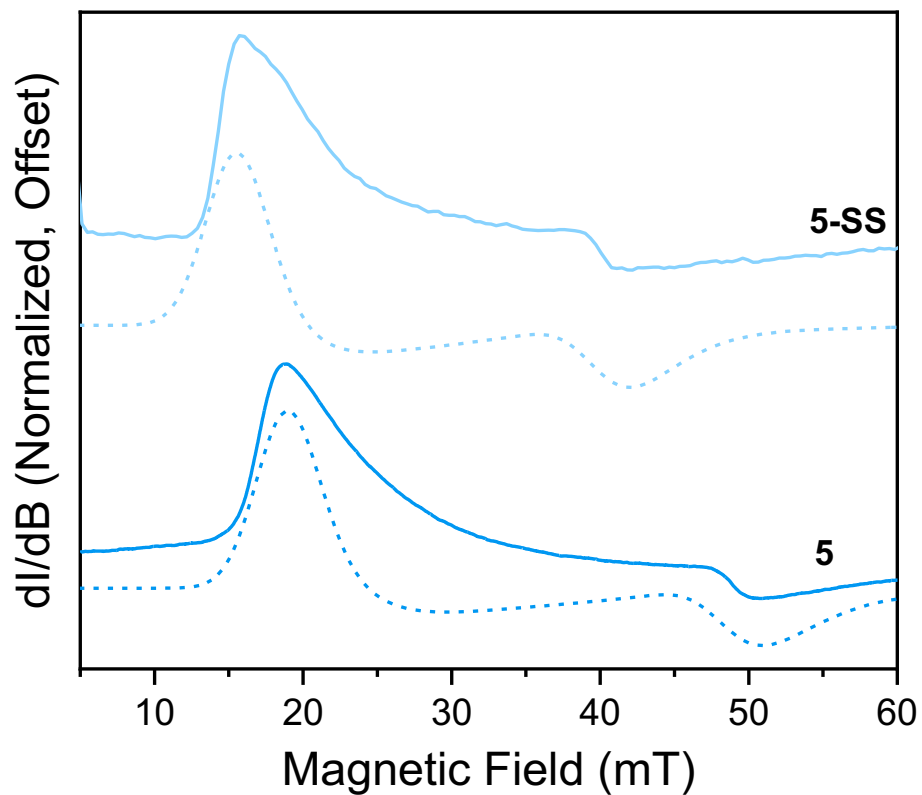


**Figure S13.** CW L-band EPR spectra of **5** and **5-SS** in 30 mM frozen glass solutions of an ethylene glycol/water (1:1 v/v) solvent system at 112 K. Dashed lines below each spectrum are the simulated spectra using the parameters from Table S7. Spectra appear offset due to slightly different tuning frequencies used in each experiment (1.095 GHz for **5-SS** and 1.360 GHz for **5**).

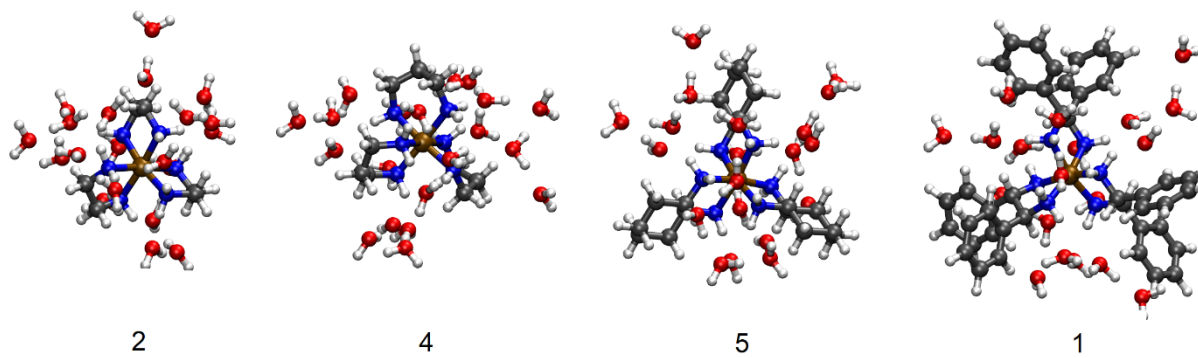


**Figure S14.** The putative global minima of the structures of the four Cr(III) complexes **1**, **2**, **4**, and **5** micro-solvated with 20 water molecules.

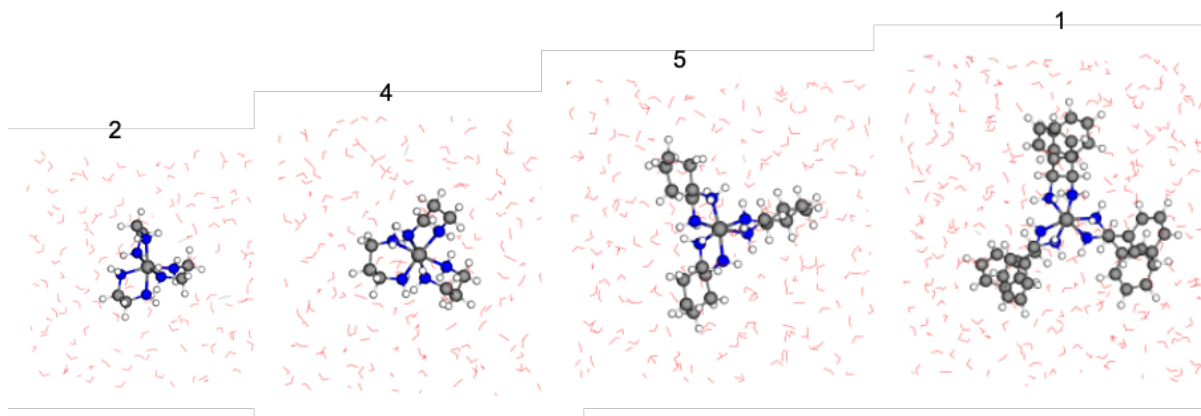


**Figure S15.** Molecular simulation boxes of the four Cr(III) complexes in water.

## References

- 1 E. Pedersen, *Acta Chem. Scand.*, 1970, **24**, 3362–3372.
- 2 R. D. Gillard, P. R. Mitchell, D. H. Busch, C. R. Sperati, H. B. Jonassen and C. W. Weston, *Inorg. Synth.*, 2007, **38**, 184–186.
- 3 G. M. SHELDRIK, *SADABS*.
- 4 G. M. Sheldrick, *Acta Crystallogr. Sect. Found. Adv.*, 2015, **71**, 3–8.
- 5 G. M. Sheldrick, *Acta Crystallogr. Sect. C Struct. Chem.*, 2015, **71**, 3–8.
- 6 G. M. Sheldrick, *Acta Crystallogr. A*, 2008, **64**, 112–122.
- 7 S. Stoll and A. Schweiger, *J. Magn. Reson.*, 2006, **178**, 42–55.
- 8 R. W. Quine, G. A. Rinard, B. T. Ghim, S. S. Eaton and G. R. Eaton, *Rev. Sci. Instrum.*, 1996, **67**, 2514–2527.
- 9 G. A. Rinard, S. S. Eaton, G. R. Eaton, C. P. J. Poole and H. A. Farach, in *Handbook of Electron Spin Resonance*, eds. C. P. J. Poole and H. A. Farach, Springer-Verlag, New York, 1999, vol. 2, pp. 1–23.
- 10 R. Bonomo and F. Riggi, *Chem. Phys.*, 1991, **151**, 323–333.
- 11 U. Casellato, R. Graziani, R. P. Bonomo and A. J. D. Bilio, *J. Chem. Soc. Dalton Trans.*, 1991, 23–31.
- 12 C. J. H. Jacobsen, E. Pedersen, H. Weihe, C. H. Petersen, J. Springborg, D.-N. Wang and S. B. Christensen, *Acta Chem. Scand.*, 1992, **46**, 928–932.
- 13 C. Legein, J. Y. Buzare, J. Emery and C. Jacoboni, *J. Phys. Condens. Matter*, 1995, **7**, 3853–3862.
- 14 J. Zhang, V.-A. Glezakou, R. Rousseau and M.-T. Nguyen, *J. Chem. Theory Comput.*, 2020, **16**, 3947–3958.
- 15 J. Zhang and M. Dolg, *Phys. Chem. Chem. Phys.*, 2015, **17**, 24173–24181.
- 16 J. Zhang and M. Dolg, *Phys. Chem. Chem. Phys.*, 2016, **18**, 3003–3010.
- 17 W. L. Jorgensen, D. S. Maxwell and J. Tirado-Rives, *J. Am. Chem. Soc.*, 1996, **118**, 11225–11236.
- 18 D. V. D. Spoel, E. Lindahl, B. Hess, G. Groenhof, A. E. Mark and H. J. C. Berendsen, *J. Comput. Chem.*, 2005, **26**, 1701–1718.
- 19 S. Alvarez, D. Avnir, M. Llunell and M. Pinsky, *New J. Chem.*, 2002, **26**, 996–1009.
- 20 S. Alvarez, P. Alemany, D. Casanova, J. Cirera, M. Llunell and D. Avnir, *Coord. Chem. Rev.*, 2005, **249**, 1693–1708.